# Influence of 3D printing process parameters and design on mechanical properties of tissue scaffolds

Karim Poonawala<sup>1</sup> and Bin Zhang<sup>1\*</sup>

<sup>1</sup>Department of Mechanical and Aerospace Engineering, Brunel University London, UB8 3PH, United Kingdom

**Abstract.** This project investigated the influence of printing process parameters on the printability and mechanical properties of bone tissue scaffolds fabricated using fused deposition modelling (FDM). Given that tissue scaffolds require specific structural and mechanical characteristics for their intended applications, the manufacturing process was examined to evaluate the effects of distinct printing parameters on the final scaffold properties. Specimens were fabricated with varying parameter values, assessed for structural integrity, and subjected to uniaxial compression testing to determine their mechanical behaviour. The results revealed that printing parameters significantly influenced both the structural quality and mechanical performance of the scaffolds, notably affecting defect formation, compressive strength, and the Young's modulus.

#### 1 Introduction

Tissue scaffolds are used for the restoration and replacement of various biological tissues, providing supporting structures upon which cells can be seeded and proliferate to form new tissue. Such scaffolds require specific structural and mechanical properties for their intended environment, which can be affected by factors such as the manufacturing process, material, and scaffold design. Fused deposition modelling (FDM) is a 3D printing technique with the advantages of low hardware and operational cost, while featuring flexibility in materials and geometries that can be produced, and has been reported as a successful process for the production of tissue scaffolds.

The fabrication of scaffolds through additive manufacturing has been reported since 2000 by Hutmacher et al. [1], with FDM emerging as a primary method [2]. Typical scaffold geometry, following the ubiquitous layer-wise approach of 3D printing, consists of layered arrangements of filaments referred to as a "laydown pattern." This approach, which limits filament orientation, results in anisotropic properties [3, 4]. Additionally, 3D printing process parameters influence the mechanical properties of the resulting constructs. It has been widely demonstrated that increasing the nozzle temperature improves mechanical properties, as reported by Spoerk et al. [5]. However, many studies investigating the effects of printing parameters on scaffold properties report conflicting findings—likely due to the complexity of the process and the difficulty in independently modifying individual parameters [4]. This challenge can be addressed by independently controlling the 3D printing code (G-code), using tools such as FullControl GCode

Designer, which allows users to define specific print paths and parameters directly [6].

This project aimed to investigate the influence of printing process parameters on the printability and mechanical properties of scaffold structures, particularly those intended for bone tissue. The study (1) analysed suitable ranges for printing process parameters to successfully produce scaffolds; (2) designed and produced scaffolds with varying characteristics, such as extrusion width and pore size, using the FDM process; and (3) evaluated the mechanical properties of the scaffolds fabricated using different printing parameters and design characteristics.

#### 2 Material and method

#### 2.1 Scaffold design

Scaffold structures were designed with careful consideration of filament arrangement, orientation, layering, and other factors to control pore architecture and overall scaffold characteristics. A "zig-zag" pattern, as shown in Figure 1, was used—consisting of longer inner filaments that formed the porous structure, interconnected by alternating outer filaments that defined the scaffold perimeter. This design provided structural reinforcement at the perimeter while maintaining lateral porosity. The scaffolds featured rectangular-shaped pores and a rectangular perimeter and were designed with a cubic structure measuring 20 mm per side. Scaffolds would typically have an organically shaped perimeter to better conform to the target anatomical site, depending on the tissue engineering application.

<sup>\*</sup> Corresponding author: bin.zhang@brunel.ac.uk

Fig. 1. Schematic diagram of the "zig-zag" filament pattern used in scaffold design.

## 2.1.1 Pore width

Pore width (or size) refers to the distance between extruded filaments, which in this study varied as 0.5, 1.0, and 1.5 mm. Increasing pore width enhances porosity but reduces overall strength and structural integrity. Isotropic properties were investigated in relation to this parameter.

#### 2.1.2 Extrusion width

Extrusion width and height refer to the cross-sectional dimensions of the extruded filament. The height determines each layer's thickness and affects the resolution of the perimeter, while the width influences the internal structure's resolution and the perimeter's thickness. In this study, extrusion height and width were kept equal to ensure a uniform cross-section; thus, the combined parameter is referred to as extrusion width. The extrusion width was varied at 0.2, 0.3, and 0.4 mm, and its influence on the isotropic behaviour of the structure was investigated.

#### 2.2 3D printing process parameters

The 3D printer used was the Prusa i3 MK3S+ (Prusa Research Ltd., Czech Republic). FullControl GCode Designer [6] was used to create the G-code for scaffold production. This approach enabled precise control over individual extrusion movements and the associated printing parameters—capabilities not achievable with standard slicer software. Repetier-Host [7], an open-source 3D printing application, was used in tandem to preview and analyse the G-code output. Polylactic Acid (PLA) was chosen for this investigation due to its ubiquity, biodegradability, and biocompatibility. A baseline value was established and maintained for each parameter as a control while other parameters were varied.

#### 2.2.1 Printing speed

Printing speed was varied to optimise both product quality and the fabrication process. It defines the speed at which the print head moves while extruding. Printing speeds of 1000, 1500, and 2000 mm/min were investigated to assess their influence on the mechanical properties in the vertical (Z) direction as shown in Figure 2.

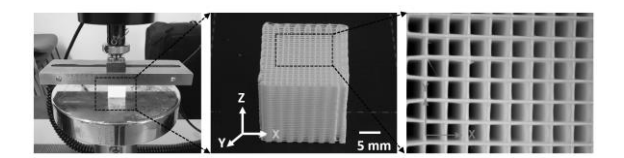


Fig. 2. 3D-printed scaffold specimen with 0.3 mm extrusion width and 2.0 mm pore width, subjected to compression testing in the vertical (Z) direction.

#### 2.2.2 Nozzle temperature

The nozzle temperature dictates the degree to which the input filament is heated and melted, typically following the manufacturer's recommendation for PLA, the nozzle temperature ranges from 200 to 220 °C, and the bed temperature is 60 °C [8]. Lower temperatures can hinder adhesion, while higher temperatures may result in overextrusion. Nozzle temperatures of 200, 210, and 220 °C were investigated to assess their influence on the mechanical properties.

#### 2.2.3 Extrusion multiplier

The extrusion multiplier (also called flow rate in slicing software) is a configurable setting in 3D printing. In FDM printing, the printer extrudes material by dispensing the amount of filament specified in the G-code during each movement. In both slicer and FullControl software, this extrusion value is automatically calculated; however, it can be manually adjusted by changing the extrusion multiplier.

#### 2.3 Mechanical testing

Uniaxial compressive testing was performed using a ZwickRoell universal testing machine (ZwickRoell Ltd, UK). Scaffolds were tested in three orthogonal directions to assess isotropic behaviour for various geometry parameters, such as pore width and extrusion width. For printing parameters—such as printing speed, nozzle temperature, and extrusion multiplier—testing was conducted along the Z direction. The testing setup is shown in Figure 2. Testing procedures and conditions followed ISO 844 Rigid Cellular Plastics [9], with tests conducted at a speed of 2 mm/min up to 20% deformation. All tests were performed in triplicate.

## 3 Results and discussion

### 3.1 Pore width

Scaffolds with pore widths of 0.5, 1.0, and 1.5 mm were successfully produced, and their mechanical properties were tested to assess isotropic behaviour under three orthogonal directions: X, Y, and Z. Detailed data for the X, Y, and Z directions at each pore width are presented in Table 1. Figure 3(a) shows the stress—strain plots of scaffolds under uniaxial compression in different directions for a pore width of 1.0 mm. The results show that the specimens exhibited the highest yield strengths

and Young's modulus in the Y direction, followed by the X, and then the Z direction. Compression along the Z direction did not exhibit a distinct ultimate strength; instead, stress continued to increase with deformation, indicating resistance to failure.

**Table 1.** Mechanical properties of scaffolds of varying pore width.

Pore width (mm)	Dire- ction	Yield strength (MPa)	Young's modulus (MPa)	Ultimate strength (MPa)
0.5	X	$7.86 \pm 0.16$	$1.35 \pm 0.07$	$8.64 \pm 0.47$
	Y	$8.27 \pm 0.48$	$1.67 \pm 0.04$	$9.19 \pm 1.16$
	Z	$6.04 \pm 0.27$	$1.29 \pm 0.06$	N/A
1.0	X	$3.73 \pm 0.14$	$0.93 \pm 0.08$	$3.93 \pm 0.10$
	Y	$3.32 \pm 0.51$	$1.13 \pm 0.02$	$3.74\pm0.24$
	Z	$2.34 \pm 0.03$	$0.83 \pm 0.03$	N/A
1.5	X	$1.55 \pm 0.35$	$0.62 \pm 0.09$	$2.44 \pm 0.32$
	Y	$1.90 \pm 0.01$	$0.86 \pm 0.05$	$2.34 \pm 0.07$
	Z	$1.47 \pm 0.05$	$0.65 \pm 0.03$	N/A

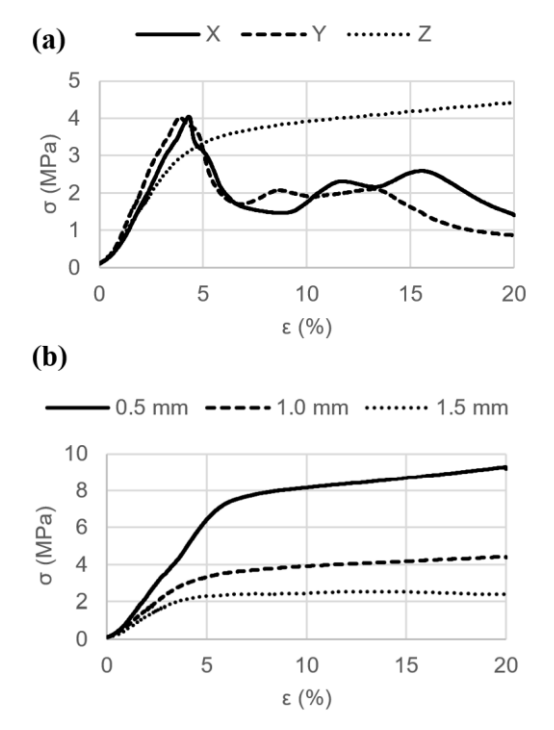


**Fig. 3.** (a) Stress-strain plots from directional compression tests on scaffolds with a pore width of 1.0 mm; (b) Stress-strain plots from Z-directional compression tests on scaffolds with varying pore widths.

Figure 3(b) shows the stress-strain plots from Z-directional compression tests on scaffolds with varying pore widths. The results indicate that mechanical performance improved as pore width decreased. When the

pore width was reduced by two-thirds, both yield strength and ultimate strength more than tripled, while the Young's modulus also increased, though to a lesser extent. The Young's modulus values for scaffolds with pore widths of 0.5, 1.0, and 1.5 mm were  $1.29 \pm 0.06$  MPa,  $0.83 \pm 0.03$  MPa, and  $0.65 \pm 0.03$  MPa, respectively. This trend is attributed to the increase in porosity associated with larger pore widths: scaffolds with pore widths of 0.5, 1.0, and 1.5 mm exhibited porosities of 62.50%, 76.92%, and 83.33%, respectively. Higher porosity typically results in reduced material density and mechanical strength.

#### 3.2 Extrusion width

Scaffolds with extrusion widths of 0.2, 0.3, and 0.4 mm were fabricated, and their mechanical properties were tested to assess isotropic behaviour along the three orthogonal directions: X, Y, and Z. Detailed data for each direction at each extrusion width are presented in Table 2.

**Table 2.** Mechanical properties of scaffolds varying in extrusion width.

Extrusion width (mm)	Dire- ction	Yield strength (MPa)	Young's modulus (MPa)	Ultimate strength (MPa)
	X	$0.81 \pm 0.12$	$0.25\pm0.07$	N/A
0.2	Y	$1.12 \pm 0.30$	$0.26\pm0.05$	N/A
	Z	$1.34 \pm 0.10$	$0.53 \pm 0.07$	N/A
	X	$3.73 \pm 0.14$	$0.93 \pm 0.08$	$3.93 \pm 0.10$
0.3	Y	$3.32 \pm 0.51$	$1.13 \pm 0.02$	$3.74 \pm 0.24$
	Z	$2.33 \pm 0.03$	$0.83 \pm 0.03$	N/A
	X	$4.67 \pm 0.08$	$0.87 \pm 0.06$	$4.93 \pm 0.08$
0.4	Y	$5.89 \pm 0.28$	$1.10 \pm 0.06$	$6.32 \pm 0.47$
	Z	$4.39 \pm 0.13$	$0.68 \pm 0.02$	N/A

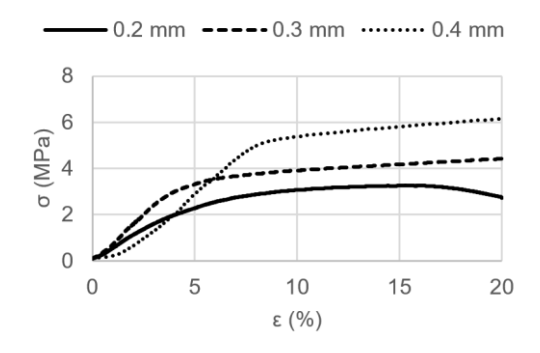


**Fig. 4.** Stress-strain plots for Z-directional compression were performed on scaffolds with varying extrusion widths.

Scaffolds produced with an extrusion width of 0.2 mm exhibited irregularities in their internal structure and poor edge adhesion, while widths of 0.5 mm and above resulted in chaotic filament deposition. Specimens with an

extrusion width of 0.4 mm demonstrated the strongest mechanical performance generally, exhibiting the highest yield and ultimate strengths, particularly in the Y direction. Figure 4 shows the stress-strain plots of scaffolds with varying extrusion widths under Zdirectional compression. The results indicate that the scaffold with an extrusion width of 0.3 mm had the highest Young's modulus, measured at  $0.83 \pm 0.03$  MPa, compared to  $0.53 \pm 0.07$  MPa for 0.2 mm and  $0.68 \pm 0.02$ MPa for 0.4 mm. The corresponding porosities for scaffolds with extrusion widths of 0.2, 0.3, and 0.4 mm were 83.33%, 76.92%, and 71.43%, respectively.

## 3.3 Printing speed

Scaffolds were fabricated using 3D printing at speeds of 1000, 1500, and 2000 mm/min, and their mechanical properties were investigated. Figure 5(a) shows the stressstrain plots for Z-directional compression of scaffolds produced at varying printing speeds. The results indicate that increasing the printing speed led to a higher prevalence of defects, and the internal cellular structure became less uniform.

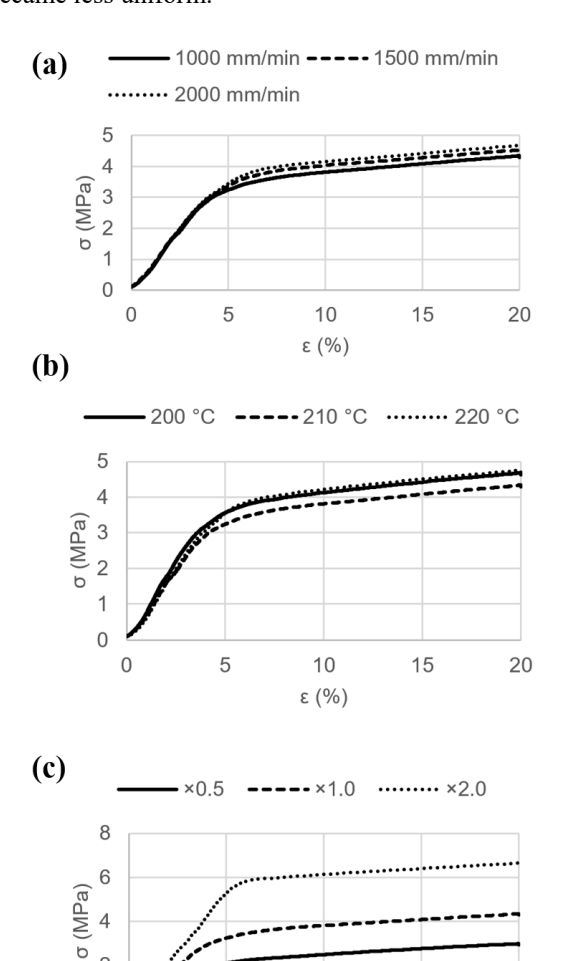


Fig. 5. Stress-strain plots for Z-directional compression performed on scaffolds produced with varying (a) printing speeds, (b) nozzle temperatures, and (c) extrusion multipliers.

10

ε (%)

15

20

5

2

0

0

#### 3.4 Nozzle temperature

Varying nozzle temperatures of 200, 210, and 220 °C were applied during 3D printing. Figure 5(b) shows the stress-strain plots for Z-directional compression of scaffolds produced at these different temperatures. The results indicate that, although the printed geometries did not show any visible differences, the yield strength varied, as did the Young's modulus. As shown in Table 3, the scaffolds fabricated at 200, 210, and 220 °C exhibited yield strengths of  $2.69 \pm 0.07$  MPa,  $2.58 \pm 0.08$  MPa, and  $2.66 \pm 0.05$  MPa, respectively, demonstrating the most desirable properties at the lowest temperature of 200 °C.

Table 3. Mechanical properties of scaffolds produced with varying printing speeds, nozzle temperature, and extrusion multiplier.

Parameter		Yield strength (MPa)	Young's modulus (MPa)	
; 1)	1000	$2.49 \pm 0.24$	$0.78 \pm 0.06$	
Printing speed (mm/min)	1500	$2.53\pm0.03$	$0.79 \pm 0.01$	
w) s	2000	$2.63\pm0.01$	$0.78 \pm 0.03$	
ure	200	$2.69 \pm 0.07$	$0.86 \pm 0.04$	
Nozzle temperature (°C)	210	$2.58 \pm 0.08$	$0.78 \pm 0.06$	
ten	220	$2.66\pm0.05$	$0.82\pm0.03$	
on er	0.5	$1.39\pm0.02$	$0.53\pm0.01$	
Extrusion multiplier	1.0	$2.58 \pm 0.08$	$0.78 \pm 0.06$	
	1.5	$5.12 \pm 0.27$	$1.11 \pm 0.04$	

#### 3.5 Extrusion multiplier

The extrusion multiplier is a scaling factor that determines how much filament is extruded during printing. A multiplier of 1.0 (or 100%) means the printer extrudes exactly the amount calculated by the slicing software. A value of 1.5 instructs the printer to extrude more filament (over-extrusion), while a value of 0.5 reduces the extrusion amount (under-extrusion). Figure 5(c) shows the stress-strain plots for Z-directional compression of scaffolds produced with varying extrusion multipliers:  $\times 0.5$ ,  $\times 1.0$ , and  $\times 1.5$ . The results demonstrate that the extrusion multiplier significantly impacts visual and mechanical properties, with over-extrusion appearing to improve print quality. The Young's modulus for extrusion multipliers of  $\times 0.5$ ,  $\times 1.0$ , and  $\times 1.5$  were  $0.53 \pm 0.01$  MPa,  $0.78 \pm 0.06$  MPa, and  $1.11 \pm 0.04$  MPa, respectively. Yield strength increased in a similar trend, indicating that higher extrusion multipliers enhance the mechanical integrity of the printed scaffolds.

# 4 Conclusions

This project clearly demonstrated the influence of 3D printing process parameters on scaffold printability and mechanical properties. Process parameters were found to significantly affect printability, with extrusion width having the most pronounced impact. Mechanical properties were also strongly influenced, with most parameters showing a clear relationship with scaffold strength. Among the parameters tested, pore width had the greatest effect on mechanical performance. Due to the characteristics of FDM 3D printing and the scaffold designs used, anisotropic behaviour was observed.

Nozzle temperature and printing speed had relatively minor and negligible effects, respectively. Future experiments could explore more extreme values—particularly higher printing speeds that align more closely with those commonly used in slicer software. While this study focused on scaffold structures with rectangular-shaped pores and perimeters, previous work suggests that designs with more complex or higher-sided pore geometries may offer improved mechanical performance. Investigating such alternative designs could help evaluate the trade-offs and potential benefits of more advanced scaffold architectures.

In general, the scaffolds in this study were designed using a consistent, regular "zig-zag" pattern. This pattern enabled the formation of rectangular pores and allowed both design and printing parameters to be easily adjusted without altering the overall geometry. The design also made defects more easily detectable and facilitated straightforward calculations of density and porosity. The selected range of extrusion widths remained within the established printing capabilities of the system, while nozzle temperature values were limited to those recommended by the filament manufacturer. This ensured that material behaviour could be investigated within a safe and practical range. This work provides a useful foundation for the development of robust design and 3D printing methodologies for tissue scaffold fabrication, particularly in the context of personalised medical devices.

## References

- 1. D.W. Hutmacher, Scaffolds in tissue engineering bone and cartilage. Biomaterials. **21**, 2529-2543 (2000). <a href="https://doi.org/10.1016/S0142-9612(00)00121-6">https://doi.org/10.1016/S0142-9612(00)00121-6</a>
- A. Gleadall, D. Visscher, J. Yang, D. Thomas, J. Segal, Review of additive manufactured tissue engineering scaffolds: relationship between geometry and performance. Burns & Trauma. 6 (2018). https://doi.org/10.1186/s41038-018-0121-4
- 3. I. Zein, D.W. Hutmacher, K.C. Tan, S.H. Teoh, Fused deposition modeling of novel scaffold architectures for tissue engineering applications. Biomaterials. **23**, 1169-1185 (2002). https://doi.org/10.1016/S0142-9612(01)00232-0
- 4. J. Allum, A. Gleadall, V.V. Silberschmidt, Fracture of 3D-printed polymers: Crucial role of filament-scale geometric features. Eng. Fract. Mech. **224**,

- 106818 (2020). https://doi.org/10.1016/j.engfracmech.2019.106818
- M. Spoerk, F. Arbeiter, H. Cainer, J. Sapkota, C. Holzer, Parametric optimization of intra- and interlayer strengths in parts produced by extrusion-based additive manufacturing of poly(lactic acid). J of Applied Polymer Sci. 134, 45401 (2017). https://doi.org/10.1002/app.45401
- 6. A. Gleadall, FullControl GCode Designer: Open-source software for unconstrained design in additive manufacturing. Addit. Manuf. **46**, 102109 (2021). <a href="https://doi.org/10.1016/j.addma.2021.102109">https://doi.org/10.1016/j.addma.2021.102109</a>
- 7. Hot-World GmbH & Co. KG, Repetier Software. (2025). <a href="https://www.repetier.com/">https://www.repetier.com/</a> (Accessed 30/05/2025).
- 8. Verbatim, PLA Filament. (2025). <a href="https://docs.rs-online.com/7a50/A700000012862507.pdf">https://docs.rs-online.com/7a50/A700000012862507.pdf</a> (Accessed 30/05/2025)
- 9. Rigid cellular plastics Determination of compression properties, ISO 844:2021 (2021).
- A.A. Ansari, M. Kamil, Effect of print speed and extrusion temperature on properties of 3D printed PLA using fused deposition modeling process.
  Mater. Today: Proc. 45, 5462-5468 (2021). <a href="https://doi.org/10.1016/j.matpr.2021.02.137">https://doi.org/10.1016/j.matpr.2021.02.137</a>
- S. Jaganathan, R. Kandasamy, R. Venkatachalam, M. Gunalan, R. Dhairiyasamy, Advances in optimizing mechanical performance of 3D-printed polymer composites: A microstructural and processing enhancements review. Adv. Polym. Tech. 2024, 3168252 (2024). https://doi.org/10.1155/2024/3168252